Building an appropriate active site motif into a hydrogen evolution catalyst with thiomolybdate $[Mo_3S_{13}]^{2-}$ clusters

Jakob Kibsgaard[1,2], Thomas F. Jaramillo[2] and Flemming Besenbacher[1,*]

[1]Interdisciplinary Nanoscience Center (iNANO) and Department of Physics and Astronomy,

Aarhus University, DK-8000 Aarhus C, Denmark

[2]Department of Chemical Engineering, Stanford University, Stanford, California 94305, USA

*e-mail: fbe@inano.au.dk

ABSTRACT

Identifying and understanding the active sites responsible for reaction turnover is critical to developing improved catalysts. For the hydrogen evolution reaction (HER), MoS_2 has been identified as an active non-noble metal-based catalyst. However, only edge sites turnover the reaction whereas the basal planes are catalytically inert. In an effort to develop a scalable HER catalyst with an increased number of active sites, herein we report on a Mo-S catalyst – supported thiomolybdate $[Mo_3S_{13}]^{2-}$ nanoclusters – in which most sulfur atoms in the structure exhibit a structural motif similar to that observed at MoS_2 edges. Supported sub-monolayers of $[Mo_3S_{13}]^{2-}$ nanoclusters exhibited excellent HER activity and stability in acid. Imaging at the atomic scale with scanning tunneling microscopy allowed for direct characterization of these supported catalysts. The $[Mo_3S_{13}]^{2-}$ nanoclusters reported herein demonstrated excellent turnover frequencies; higher than those observed for other non-precious catalysts synthesized by a scalable route.

KEYWORDS

Electrocatalysis, Hydrogen evolution, HER, $[Mo_3S_{13}]^{2-}$, thiomolybdate, molybdenum sulfide

MANUSCRIPT TEXT

In modern industry, molecular hydrogen (H_2) is a crucial chemical feedstock with a production rate at the global-scale of approximately 50 billion kg/yr, used primarily in petroleum refining and in the synthesis of NH_3 for fertilizer.[1] The demand for H_2 is likely to continue to increase as petroleum feedstocks are getting heavier and as the global population continues to increase. Hydrogen has also been proposed as a major energy carrier for the future.[2, 3] Today, however, hydrogen is mainly produced from steam reforming of natural gas and hence contributes to the global CO_2 emission.[1-3] It is widely believed that electrocatalysis can play a key role in next generation sustainable energy conversion technologies and as such significant attention has been devoted to clean hydrogen production through electrocatalytic processes such as photoelectrochemical (PEC) water splitting or electrolysis coupled to renewable energy sources.[4-6]

The hydrogen evolution reaction (HER, $2H^+ + 2e^- \rightarrow H_2$) constitutes half of the water splitting reaction; active catalysts are required to increase process efficiency by minimizing the overpotential needed to drive the HER. Platinum is currently the best known catalyst for the HER as it requires negligible overpotential even at high reaction rates, but the scarcity and high cost of Pt limits its widespread technological use. Non-noble metal alternatives include nickel and nickel alloy catalysts but their use is typically restricted to alkaline solutions due to corrosion issues in acidic solutions.[7-9]

Recently, biomimetic electrocatalysts based on low-cost earth-abundant first-row transitions metals have been employed for various electrocatalytic reactions including HER. Hydrogenase and nitrogenase enzymes are nature's effective HER catalysts with active centers consisting of Fe, Ni and Mo. Hinnemann *et al.* reported that undercoordinated sulfur atoms at the edges of MoS_2 have very similar

properties as the active enzymatic centers[10] and indeed nanoparticles of MoS_2 were shown to be excellent HER catalysts.[11] However, only the edges of MoS_2 nanoparticles are active, whereas the (0001) basal planes of MoS_2 are catalytically inert, and high HER activity thus requires MoS_2 nanocatalysts with a high number of exposed edge sites. Several molybdenum sulfide systems have been synthesized including molecular[12], nanoparticulate[11, 13, 14], nanowires[15], mesoporous[16], and amorphous films[17, 18]. Molecular complexes have also been studied as an intriguing class of HER catalysts, including biomimetic nickel and cobalt complexes[19-22] and polyoxometalates.[23, 24] Many molecular electrocatalysts, however, have been found to be stable only in nonaqueous solvents or require very large overpotentials to achieve appreciable turnover frequencies.[25]

Herein, we report on the development of a new and interesting molecular HER catalyst, thiomolybdate $[Mo_3S_{13}]^{2-}$ nanoclusters that, upon supporting onto carbon electrode surfaces, bridges molecular and solid state electrocatalysis. The $[Mo_3S_{13}]^{2-}$ nanoclusters are prepared by straightforward wet chemical methods that can readily be scaled. The clusters contain 3 different types of sulfur ligands, all intrinsically located as edge sulfur atoms, see Figure 1a, and can be viewed as molybdenum sulfide with a significant fraction of active sites as nearly all the sulfur atoms have the appropriate atomic structure for effective catalysis. Indeed, compared to other molybdenum sulfide based HER catalysts – which are the best known non-precious metal HER catalysts in strong acids – our measurements show that the $[Mo_3S_{13}]^{2-}$ nanoclusters exhibit unprecedented turnover frequencies for the HER among non-precious metal based catalysts synthesized by scalable routes. Moreover the thiomolybdate $[Mo_3S_{13}]^{2-}$ nanoclusters can be deposited onto a wide range of electrode surfaces by means of a facile drop-casting method using methanol as a solvent. The ability to deposit onto a wide range of supports in such a straightforward manner enables ready integration of these nanoclusters onto different device architectures and materials for electrochemical applications.

RESULTS AND DISCUSSION

Synthesis.

The thiomolybdate, $(NH_4)_2Mo_3S_{13}\cdot H_2O$, were prepared by reacting $(NH_4)_6Mo_7O_{24}\cdot 4H_2O$ with an ammonium polysulfide solution following the method outlined by Müller *et al.*[26] (see below for details). The synthesis yields dark red crystals (Figure 1b) which we examined by powder X-ray diffraction (XRD). The XRD pattern (Figure 1c) was found to be in agreement with experimental and simulated powder XRD patterns of $(NH_4)_2Mo_3S_{13}\cdot H_2O$ found in the literature and the corresponding crystal structure is shown in Figure 1d.[27, 28] The $(NH_4)_2Mo_3S_{13}\cdot H_2O$ was redispered in methanol (Ultraviolet-visible transmission measurements shown in Supplementary Figure S1) which facilitates cluster deposition onto any support by a simple drop-casting procedure.

To investigate the $[Mo_3S_{13}]^{2-}$ clusters and their activity for the HER we selected two different supports: highly orientated pyrolytic graphite (HOPG, Structure Probe, Inc., grade SPI-2), and high surface area graphite paper (GP, Toray TGP-60, Alfa Aesar GmbH & Co. KG). The latter was selected since the high surface area allows for higher loadings of $[Mo_3S_{13}]^{2-}$ clusters, and is a support commonly employed in commercial electrochemical devices such as water electrolyzers and fuel cells. However, the simple drop-casting deposition enables the use of a wide range of different supports materials (see Supplementary Figure S2, for examples of an oxide support and a metal support).

Characterization.

In both electrocatalysis and catalysis, it is generally difficult of estimate the number active sites.[29-31] First of all catalysis is an intrinsically local effect related to active sites on the catalyst surface. Moreover, the active sites often have special local structure and stoichiometry such as edges, corners or other defect sites, which can be extremely difficult to detect by means of most materials characterization techniques as information is often averaged over the sample surface or bulk. To investigate the intrinsic

structure and activity of individual $[Mo_3S_{13}]^{2-}$ clusters we turned to scanning tunneling microscopy (STM) which offers a means to image the clusters with atomic resolution and hence allow for direct counting of the number of active sites.[31] HOPG was chosen as support material because it exhibits atomically flat terraces that typically extend over several hundred nanometers allowing for atom-resolved imaging by STM. As carbon is electrochemically inert in the potential window under investigation, both the GP and the HOPG supports allow the activity of the $[Mo_3S_{13}]^{2-}$ clusters to be clearly distinguished from the substrate. However, in the case of HOPG the strong two-dimensional bonding within the graphite layers together with an inherently low density of surface defects result in weak bonding of adsorbates on the freshly cleaved, pristine HOPG surface. To increase the strength of adsorption we activated the freshly cleaved HOPG surface by electrochemical anodization which introduces functional groups such as –OH and –COOH, causing light pitting of the HOPG surface; these features serve as anchoring points for the $[Mo_3S_{13}]^{2-}$ clusters. The anodization was performed in a phosphate buffer (pH 7) at 1.65 V vs. Ag|AgCl for 2 min. Figure 2a shows an STM image of the anodized HOPG surface with increased surface roughness. A further zoom-in in Figure 2b shows the distorted atomic structure of the activated surface, which provides anchoring sites for the $[Mo_3S_{13}]^{2-}$ clusters. HOPG substrates were prepared by this anodization process, followed by a rinse with Millipore water (18.2 MΩ·cm) and drying in an N_2 stream. Immediately after, a 5 µl solution of 50 µM $[Mo_3S_{13}]^{2-}$ in methanol was drop-cast onto the surface. Before drying out, the solution was rinsed off by 200 µl of methanol to prevent bulk deposition and ensure only a sub-monolayer coverage of $[Mo_3S_{13}]^{2-}$ clusters on the surface.

Figure 2c shows an STM image of $[Mo_3S_{13}]^{2-}$ clusters supported onto HOPG at sub-monolayer coverage; a number of uniform, nanometer-sized bright protrusions are clearly observed. Zooming in on one of the bright features reveals an ordered atomic-scale structure. The observed seven bright

protrusions arranged in a hexagonal pattern with one in the center represents the expected symmetry pertaining to the structure of a single $[Mo_3S_{13}]^{2-}$ cluster consisting of 3 terminal S_2^{2-}, 3 bridging S_2^{2-}, and 1 central apical S, see Figure 2d. The bright spots arranged in a hexagonal pattern could represent either the interstitial spaces between the sulfur dimers or the sulfur dimers themselves, as sulfur atoms have been commonly imaged in previous STM studies of MoS_2.[32-34] Ultimately, STM images show that we have highly dispersed individually separated $[Mo_3S_{13}]^{2-}$ clusters on the surface. Overview images such as the one shown in Figure 2c offer a quantitative measure of the surface coverage, which was determined to be ~8 (±2) × 10^{12} $[Mo_3S_{13}]^{2-}$ clusters per cm^2 HOPG.

The chemical nature of the sub-monolayer $[Mo_3S_{13}]^{2-}$|HOPG sample was investigated by X-ray photoelectron spectroscopy (XPS) (Figure 3). Each element has characteristic binding energies associated with electronic transitions from each of its core atomic orbitals, which together with small shifts from the chemical environment gives rise to a characteristic set of peaks in XPS. Deconvolution of the Mo 3d region by peak fitting reveal a single Mo 3d doublet at a position indicative of Mo with a 4+ oxidation state. A broad S 2s feature was observed near the Mo $3d_{5/2}$ peak, indicating multiple chemical states of sulfur. For further analysis, we examined the S 2p region which was fitted with three distinct doublets ($2p_{3/2}$,$2p_{1/2}$): (a) one doublet at (162.3 eV, 163.5 eV) arising from the terminal S_2^{2-} ligands, (b) one doublet at (163.6 eV, 164.8 eV) reflecting the bridging S_2^{2-} ligands and the apical S^{2-} ligand of the $[Mo_3S_{13}]^{2-}$ clusters, and (c) a doublet at even higher binding energies (164.3 eV, 165.5 eV) accounting for residual sulfur from the polysulfide solution. The highest binding energy doublet, however, decreases or completely disappears after HER studies (see Supplementary Figure S3) indicating a removal of residual polysulfides from the surface during catalyst testing. Regarding the XPS spectra pertaining to the thirteen S atoms in the $[Mo_3S_{13}]^{2-}$ cluster, the ratio of the higher binding energy doublet to the lower binding energy doublet is 7:6, as expected. These observations are in

agreement with previous XPS studies of $[Mo_3S_{13}]^{2-}$ and indicate that the chemical state of the cluster has not changed after deposition onto the electrode surface.[35, 36]

Catalytic activity.

The catalytic activity of the $[Mo_3S_{13}]^{2-}$ clusters was evaluated for the hydrogen evolution reaction (HER) using a three-electrode electrochemical cell. Figure 4a shows iR-corrected linear sweep voltammograms in the cathodic direction for the bare anodized HOPG surface compared to that with supported $[Mo_3S_{13}]^{2-}$ clusters, normalized to the projected geometric area of the electrode (conditions: N_2-purged 0.5 M H_2SO_4 (aq), 23 °C, sweep rate 5 mV/s). The bare anodized HOPG surface shows no HER activity in the investigated potential window, only a reduction peak around -0.10 V vs RHE which we associate with the functionalized surface since this peak is absent in sweeps of freshly cleaved pristine HOPG surfaces (data not shown). The $[Mo_3S_{13}]^{2-}$|HOPG sample on the other hand shows a sharp, exponential increase in the magnitude of the cathodic current density with increasing overpotential, indicative of HER activity. The reduction peak associated with the functionalized HOPG surface is only faintly present as many of these sites are covered with adsorbed $[Mo_3S_{13}]^{2-}$ clusters. Figure S4 shows a large scale STM image of $[Mo_3S_{13}]^{2-}$ clusters after electrochemical HER testingand the uniform, nanometer-sized bright protrusions are still clearly observed, indicating that the $[Mo_3S_{13}]^{2-}$ clusters have not sintered nor have they condensed into larger islands, e.g. of MoS_2.

The HER activity of $[Mo_3S_{13}]^{2-}$ was further evaluated by depositing the clusters onto graphite paper (GP) disks at higher loadings for a more direct comparison to literature data on other molybdenum sulfide HER catalysts. Samples of 10, 20, 50, and 100 μg $[Mo_3S_{13}]^{2-}$ per cm^2 were deposited by drop-casting a solution of 1 mM $[Mo_3S_{13}]^{2-}$ in methanol (close to saturation, higher concentrations can be achieved by using other solvents, e.g. DMSO). The graphite paper disks were inserted into the electrolyte by means of an insulated wire connected to the potentiostat. The HER activity of these samples is shown in Figure 4b as iR-corrected cyclic voltammograms. All four samples exhibit

excellent catalytic activity for the HER, as evidenced by a very early onset for the reaction at overpotentials of only 0.10 V – 0.12 V, and by reaching a current density of 10 mA/cm^2 at low overpotentials, between 0.18 V – 0.22 V. As expected, we see that higher loadings result in a higher current density at a given potential. The very low degree of hysteresis between the cathodic and anodic sweeps also indicates that the influence of mass transport limitations was small for this particular electrode architecture.[16]

Tafel plots of the polarization curves are shown in Figure 4c. In Tafel plots, the logarithm of the current density is plotted against the overpotential. Analyzing the Tafel slope of an electrochemical reaction, typically reported with the unit of mV per decade of current density, can help provide insight into mechanistic pathways.[37] All Tafel slopes pertaining to the $[Mo_3S_{13}]^{2-}$|GP samples are found to be 38-40 mV per decade; values similar to those found for previously studied amorphous MoS_x[13] and for MoS_2 on reduced graphene oxide[17] and may suggest a Volmer-Heyrovsky HER mechanism (see Supplementary information).[13, 17] Interestingly, we find that the Tafel slope of the sub-monolayer $[Mo_3S_{13}]^{2-}$|HOPG sample is approximately 57 mV per decade, slightly higher than that observed for the $[Mo_3S_{13}]^{2-}$|GP sample. This Tafel slope is similar to values observed on UHV prepared MoS_2 nanoparticles[11] as well as other nanostructured forms of MoS_2.[15, 16] A Tafel slope of 60 mV per decade as observed in the case of sub-monolayer coverage has been suggested to reflect a chemical rearrangement step as the rate determining step (see Supplementary information for details).[38] On the graphite paper support, the lower Tafel slope (ca. 40 mV per decade) could result in a change in mechanism due to the considerably higher loading of $[Mo_3S_{13}]^{2-}$ clusters, where the closer proximity of active sites could affect the bonding of intermediates and the reaction mechanism, e.g. the electrochemical desorption (Heyrovsky) could become rate determining. To examine whether or not the $[Mo_3S_{13}]^{2-}$ clusters could condense into different phase at higher coverage, e.g. MoS_2, which could impact the Tafel slope, we performed Raman spectroscopy before and after HER testing (see

Supplementary Figure S7). Raman spectroscopy probes the vibrational modes of chemical bonds and therefore provides a fingerprint spectrum that can be used to identify chemical compounds. We observed no change in the characteristic $[Mo_3S_{13}]^{2-}$ Raman spectrum upon HER cycling and we therefore conclude that the $[Mo_3S_{13}]^{2-}$ clusters do not change structure or composition during the HER.

Turnover frequency.

In catalysis, the best figure of merit to use in comparing activities among different catalyst materials is by means of their turnover frequency (TOF).[29] For MoS_2 it is well established that only edge sites are catalytically active. For TOF normalization, we calculate the TOF per surface exposed Mo site in order to avoid difficulties in distinguishing the activity of different sulfur edge sites present in the $[Mo_3S_{13}]^{2-}$ clusters as well as those within other molybdenum sulfide HER catalysts. A direct calculation of the TOF of the $[Mo_3S_{13}]^{2-}$ clusters per Mo atom was determined by normalizing the HER current density from the polarization curves to 3 times the surface density of $[Mo_3S_{13}]^{2-}$ clusters as calculated by mass loading or by direct measurements using STM images in the case of the $[Mo_3S_{13}]^{2-}$|HOPG sample. For the purpose of direct comparison, Figure 4d displays the TOFs of the $[Mo_3S_{13}]^{2-}$ clusters from the two types of samples described in this work, the $[Mo_3S_{13}]^{2-}$|HOPG sample and the four different samples of $[Mo_3S_{13}]^{2-}$|GP (with loadings of 10, 20, 50, and 100 μg/cm^2), along with seven state-of-the-art molybdenum sulfides published in the recent literature. These include: MoO_3-MoS_2 core-shell nanowires,[15] a mesoporous MoS_2 with a double-gyroid morphology,[16] MoS_2 nanoparticles supported onto reduced graphene oxide (RGO),[13] electrodeposited amorphous MoS_3,[17] a wet-chemically prepared amorphous MoS_x,[18] $[Mo_3S_4]^{4+}$ cubanes supported onto HOPG,[39] and ultra-high vacuum (UHV) deposited MoS_2 nanoparticles supported onto Au(111).[11] Figure 4d plots TOFs in the potential range where the current densities fall within the Tafel region and hence the reaction is expected to be controlled by electrode kinetics and not by other limitations, e.g. mass transport. The Supplementary Information contains further details on TOF calculations.

All forms of nanostructured molybdenum sulfides plotted in Figure 4d exhibit high catalytic activity for the HER, though some forms are more active than others. On a TOF basis, the most active molybdenum sulfide HER catalyst ever demonstrated consists of UHV-deposited MoS_2 nanoparticles on Au(111).[11] The edge sites of these UHV MoS_2 nanoparticles exhibit TOFs (per edge site) of 1 s^{-1} and 10 s^{-1} at overpotentials of approximately 0.10 V and 0.16 V, respectively. This sets the benchmark for HER catalysis on MoS_2. In comparison, the sub-monolayer $[Mo_3S_{13}]^{2-}$|HOPG sample also exhibits extremely high catalytic activity, as evidenced by a TOF (per Mo atom) of 3 s^{-1} at an overpotential of 0.20 V. While not quite as active as the UHV-prepared MoS_2 nanoparticles, the $[Mo_3S_{13}]^{2-}$|HOPG sample has advantages in that the synthesis route is more scalable (liquid drop-casting vs. UHV deposition) and the clusters are anchored much more strongly to the support. Figure 4d also reveals that apart from the UHV-prepared MoS_2 nanoparticles, the $[Mo_3S_{13}]^{2-}$|HOPG TOF is much higher than all the other molybdenum sulfide catalysts by roughly an order of magnitude. These measurements on the sub-monolayer $[Mo_3S_{13}]^{2-}$|HOPG sample likely sets the upper limit for the TOF of $[Mo_3S_{13}]^{2-}$ clusters as the majority of active sites are likely accessible due to the exposure of every cluster to the electrolyte. Accordingly, we observe that the TOFs (per Mo atom) of the higher loading $[Mo_3S_{13}]^{2-}$|GP samples are a factor of 5 lower than the sub-monolayer $[Mo_3S_{13}]^{2-}$|HOPG sample. We attribute the lower TOF to aggregation of the clusters which prevents some clusters from participating in the reaction. It is important to note that for the $[Mo_3S_{13}]^{2-}$ samples as well as for the MoS_2|RGO sample, we assume that all Mo atoms loaded onto the electrode are 'surface atoms' for the sake of TOF normalization. For the other molybdenum sulfides catalysts plotted in Figure 4d, we explicitly calculate the fraction of Mo atoms that should be taken into account as 'surface atoms' for the TOF calculations. The TOF of those catalysts would consequently diminish if all Mo atoms were taken into account, e.g. TOF calculations for the MoO_3-MoS_2 core-shell nanowires assume that only 1 out of 5 Mo atoms are located at the surface, based on TEM imaging.[15] In any event, the $[Mo_3S_{13}]^{2-}$|GP samples outperform most of these

nanostructured molybdenum sulfide HER catalysts. We suggest that the origin of the extremely high TOF is related to the fact that most sulfur sites on the cluster exhibit similarities to the MoS_2 edge structure that is known to be catalytically active.

Stability.

Stability is an important concern for all catalysts. To assess the HER stability of the $[Mo_3S_{13}]^{2-}$ clusters we measured 1,000 continuous cyclic voltammograms for a $[Mo_3S_{13}]^{2-}$|GP sample with a loading of 50 μg $[Mo_3S_{13}]^{2-}$ per cm^2 between -0.3 and 0.2 V vs RHE (not iR-corrected) at 100 mV/s. This replicates the diurnal cycling experienced by a HER catalyst for solar water splitting. The lower limit was selected according to previous accelerated HER testing[15, 40] and corresponds roughly to a current density of ~20 mA/cm^2 for a non iR-corrected device which is equivalent to ~25% efficient solar-to-hydrogen conversion efficiency in a solar water splitting device.[4] Figure 4e shows the iR-corrected cathodic-going sweep for the three particular cycles: the initial cycle (0) and after 100 and 1,000 stability cycles. We observe a slight decrease of the cathodic current density with increased potential cycling, however the sample remains highly catalytically active. The Tafel slope remains constant around ~40 mV per decade which suggests that the HER mechanism is not changed by potential cycling. Electrochemical impedance spectroscopy (EIS) measurements, however, show that the diameter of low frequency semi-circle increases with increased potential cycling (details on EIS in Supplementary information). We attribute this change to the desorption of $[Mo_3S_{13}]^{2-}$ clusters during the accelerated durability test due to rigorous H_2 bubble formation at the electrode surface, ultimately resulting in fewer sites for catalysis. However, the activity loss appears much less significant than what was observed for carbon supported $[Mo_3S_4]^{4+}$ cubanes at similar current densities.[39]

Conclusion.

Herein we report on thiomolybdate $[Mo_3S_{13}]^{2-}$ nanoclusters as a scalable, earth-abundant HER catalyst with extremely high activity and excellent stability. The catalyst is prepared by straightforward wet-

chemical methods and can be supported on a variety of substrates by simple drop-casting. We studied this catalyst supported on both high surface area graphite paper and on highly orientated pyrolytic graphite, finding that this catalyst exhibits the highest HER turnover frequency of any molybdenum sulfide catalyst ever synthesized by scalable wet-chemical methods. We attribute this high activity to the fact that these small $[Mo_3S_{13}]^{2-}$ nanoclusters inherently expose a significant number of active edge sites. The addition of promoter atoms could lead to further enhancement in the catalytic activity for the HER[41-44] and potentially enable Mo_3S_{13}-based catalyst to be able to compete against the best precious metal catalysts, e.g. Pt, available today.

Methods

Synthesis of $[Mo_3S_{13}]^{2-}$ nanoclusters:

The thiomolybdate, $(NH_4)_2Mo_3S_{13}\cdot H_2O$, was prepared by the method outlined by Müller et al.[26] In short 4.0 g of $(NH_4)_6Mo_7O_{24}\cdot 4H_2O$ (Sigma-Aldrich) was dissolved in 20 ml of water in an Erlenmeyer flask. 120 ml of an ammonium polysulfide solution (< 25 w%, Acros Organics) was added and the flask was covered with a watch glass. The solution was then kept on an oil bath (96˚C) for 5 days without stirring. Dark red crystals of $(NH_4)_2Mo_3S_{13}\cdot H_2O$ precipitated and were removed by filtering, followed by washing successively with water and ethanol. To remove excess sulfur, the $(NH_4)_2Mo_3S_{13}\cdot H_2O$ crystals were heated in hot toluene (~80 ˚C) for 2-4 hr. Finally the crystals were dried in air. The heating in toluene removes most of the residual sulfur but small a quantity is still observed in XPS (see Figure 3b). If all sulfur residues are to be removed carbon disulfide can be used. [26, 35]

Physical Characterization:

XRD was performed using a Bruker D8 Discover diffractometer using Cu Kα radiation. XPS was performed using a Kratos Axis Ultra DLD with binding energies referenced to HOPG at 284.5. Ultraviolet-visible transmission spectroscopy was performed using a Shimadzu UV-1800 spectrophotometer. Scanning tunneling microscopy was performed using an Agilent 5500 system with a dedicated high-resolution STM scanner and mechanically cut Pt-Ir (80/20) tips. Raman spectroscopy was performed using a NT-MDT NTEGRA Spectra system with a 473 nm excitation laser.

Electrochemical Characterization:

The electrochemical measurements were carried out in a standard three-electrode electrochemical setup using a μAutolab Type III/FRA2 potentiostat. The $[Mo_3S_{13}]^{2-}$|HOPG or $[Mo_3S_{13}]^{2-}$|GP samples served as the working electrode with a graphite rod as counter electrode and a Ag|AgCl reference electrode (3 M KCl, Metrohm). All cyclic voltammograms of the HER activity were conducted using a 0.5 M H_2SO_4

electrolyte under continuous sparging with N_2. The reference electrode was calibrated to the reversible hydrogen potential using platinum mesh for both the working and counter electrodes in the same 0.5 M H_2SO_4 electrolyte sparged with H_2. This calibration resulted in a shift of -0.24 V versus the RHE.

ACKNOWLEDGMENT

JK gratefully acknowledges the Carlsberg Foundation for a post-doctoral fellowship. JK and TFJ acknowledge support from the U.S. Department of Energy, Office of Science, Office of Basic Energy Sciences, under Contract No. DE-SC0008685. We thank Dr. Zhebo Chen for helpful discussion and Dr. Andrey V. Malkovskiy for assistance with Raman spectroscopy measurements.

AUTHOR CONTRIBUTIONS

JK conceived the studies. JK performed the experimental work and JK, TFJ, and FB co-wrote the paper.

ADDITIONAL INFORMATION

The authors declare no competing financial interests. Supplementary information is available.

REFERENCES.

1. U.S. Energy Information Administration. The Impact of Increased Use of Hydrogen on Petroleum Consumption and Carbon Dioxide Emissions. (2008).
2. Turner, J. A. Sustainable Hydrogen Production. *Science* **305**, 972-974 (2004).
3. Nowotny, J., Sorrell, C. C., Sheppard, L. R. & Bak, T. Solar-hydrogen: Environmentally safe fuel for the future. *Int. J. Hydrogen Energy* **30**, 521-544 (2005).
4. Chen, Z. et al. Accelerating materials development for photoelectrochemical hydrogen production: Standards for methods, definitions, and reporting protocols. *J. Mater. Res.* **25**, 3-16 (2010).
5. Walter, M. G. et al. Solar Water Splitting Cells. *Chem. Rev.* **110**, 6446-6473 (2010).
6. Cook, T. R. et al. Solar Energy Supply and Storage for the Legacy and Nonlegacy Worlds. *Chem. Rev.* **110**, 6474-6502 (2010).
7. Choquette, Y., Brossard, L., Lasia, A. & Ménard, H. Investigation of hydrogen evolution on Raney-Nickel composite-coated electrodes. *Electrochim. Acta* **35**, 1251-1256 (1990).
8. Lačnjevac, U. Č., Jović, B. M., Jović, V. D. & Krstajić, N. V. Determination of kinetic parameters for the hydrogen evolution reaction on the electrodeposited Ni–MoO_2 composite coating in alkaline solution. *J. Electroanal. Chem.* **677–680**, 31-40 (2012).
9. McKone, J. R., Sadtler, B., Werlang, C. A., Lewis, N. S. & Gray, H. B. Ni-Mo Nanopowder for Efficient Electrochemical Hydrogen Evolution. *ACS Catal.* **3**, 166-169 (2013).
10. Hinnemann, B. et al. Biomimetic Hydrogen Evolution: MoS_2 Nanoparticles as Catalyst for Hydrogen Evolution. *J. Am. Chem. Soc.* **127**, 5308-5309 (2005).
11. Jaramillo, T. F. et al. Identification of active edge sites for electrochemical H_2 evolution from MoS_2 nanocatalysts. *Science* **317**, 100-102 (2007).
12. Karunadasa, H. I. et al. A Molecular MoS_2 Edge Site Mimic for Catalytic Hydrogen Generation. *Science* **335**, 698-702 (2012).
13. Li, Y. et al. MoS_2 Nanoparticles Grown on Graphene: An Advanced Catalyst for the Hydrogen Evolution Reaction. *J. Am. Chem. Soc.* **133**, 7296-7299 (2011).
14. Xiang, Q. J., Yu, J. G. & Jaroniec, M. Synergetic Effect of MoS_2 and Graphene as Cocatalysts for Enhanced Photocatalytic H_2 Production Activity of TiO_2 Nanoparticles. *J. Am. Chem. Soc.* **134**, 6575-6578 (2012).
15. Chen, Z. et al. Core–shell MoO_3–MoS_2 Nanowires for Hydrogen Evolution: A Functional Design for Electrocatalytic Materials. *Nano Lett.* **11**, 4168-4175 (2011).
16. Kibsgaard, J., Chen, Z., Reinecke, B. N. & Jaramillo, T. F. Engineering the surface structure of MoS_2 to preferentially expose active edge sites for electrocatalysis. *Nature Mater.* **11**, 963-969 (2012).
17. Merki, D., Fierro, S., Vrubel, H. & Hu, X. L. Amorphous molybdenum sulfide films as catalysts for electrochemical hydrogen production in water. *Chem. Sci.* **2**, 1262-1267 (2011).
18. Benck, J. D., Chen, Z. B., Kuritzky, L. Y., Forman, A. J. & Jaramillo, T. F. Amorphous Molybdenum Sulfide Catalysts for Electrochemical Hydrogen Production: Insights into the Origin of their Catalytic Activity. *ACS Catal.* **2**, 1916-1923 (2012).
19. Le Goff, A. et al. From Hydrogenases to Noble Metal–Free Catalytic Nanomaterials for H_2 Production and Uptake. *Science* **326**, 1384-1387 (2009).
20. Helm, M. L., Stewart, M. P., Bullock, R. M., DuBois, M. R. & DuBois, D. L. A Synthetic Nickel Electrocatalyst with a Turnover Frequency Above 100,000 s^{-1} for H_2 Production. *Science* **333**, 863-866 (2011).
21. Andreiadis, E. S. et al. Molecular engineering of a cobalt-based electrocatalytic nanomaterial for H_2 evolution under fully aqueous conditions. *Nature Chem.* **5**, 48-53 (2013).

22. Mondal, B. et al. Cobalt Corrole Catalyst for Efficient Hydrogen Evolution Reaction from H_2O under Ambient Conditions: Reactivity, Spectroscopy, and Density Functional Theory Calculations. *Inorg. Chem.* **52**, 3381-3387 (2013).
23. Duval, S. et al. Capture of the $[Mo_3S_4]^{4+}$ Cluster within a $\{Mo_{18}\}$ Macrocycle Yielding a Supramolecular Assembly Stabilized by a Dynamic H-Bond Network. *J. Am. Chem. Soc.* **132**, 2069-2077 (2010).
24. Hijazi, A. et al. Tuning the electrocatalytic hydrogen evolution reaction promoted by $[Mo_2O_2S_2]$-based molybdenum cycles in aqueous medium. *Dalton Trans.* **42**, 4848-4858 (2013).
25. McKone, J. R., Gray, H. B. & Lewis, N. S. Will Solar-Driven Water-Splitting Devices See the Light of Day? *Chem. Mater., Article ASAP* (2013).
26. Müller, A., Krickemeyer, E., Hadjikyriacou, A. & Coucouvanis, D. in *Inorganic Syntheses*, Vol. 27. (ed. A.P. Ginsberg) 47-51 (John Wiley & Sons, Inc., 2007).
27. Müller, A., Wittneben, V., Krickemeyer, E., Bogge, H. & Lemke, M. Studies on the Triangular Cluster $[Mo_3S_{13}]^{2-}$: Electronic Structure (Xα Calculations, XPS), Crystal Structure of $(Ph_4As)_2[Mo_3S_{13}]\bullet 2CH_3CN$ and a Refinement of the Crystal Structure of $(NH_4)_2[Mo_3S_{13}]\bullet H_2O$. *Z. Anorg. Allg. Chem.* **605**, 175-188 (1991).
28. Leist, A. et al. Semiporous MoS_2 obtained by the decomposition of thiomolybdate precursors. *J. Mater. Chem.* **8**, 241-244 (1998).
29. Boudart, M. Turnover Rates in Heterogeneous Catalysis. *Chem. Rev.* **95**, 661-666 (1995).
30. Zambelli, T., Wintterlin, J., Trost, J. & Ertl, G. Identification of the "active sites" of a surface-catalyzed reaction. *Science* **273**, 1688-1690 (1996).
31. Vang, R. T., Lauritsen, J. V., Laegsgaard, E. & Besenbacher, F. Scanning tunneling microscopy as a tool to study catalytically relevant model systems. *Chem. Soc. Rev.* **37**, 2191-2203 (2008).
32. Helveg, S. et al. Atomic-scale structure of single-layer MoS_2 nanoclusters. *Phys. Rev. Lett.* **84**, 951-954 (2000).
33. Lauritsen, J. V. et al. Size-dependent structure of MoS_2 nanocrystals. *Nature Nanotech.* **2**, 53-58 (2007).
34. Sun, D. et al. An MoS_x Structure with High Affinity for Adsorbate Interaction. *Angew. Chem. Int. Ed.* **51**, 10284-10288 (2012).
35. Muijsers, J. C., Weber, T., Vanhardeveld, R. M., Zandbergen, H. W. & Niemantsverdriet, J. W. Sulfidation Study of Molybdenum Oxide Using $MoO_3/SiO_2/Si(100)$ Model Catalysts and Mo_3^{IV}-Sulfur Cluster Compounds. *J. Catal.* **157**, 698-705 (1995).
36. Weber, T., Muijsers, J. C. & Niemantsverdriet, J. W. Structure of Amorphous MoS_3. *J. Phys. Chem.* **99**, 9194-9200 (1995).
37. Lefebvre, M. in Modern Aspects of Electrochemistry, Vol. 32. (eds. B.E. Conway, J.O.M. Bockris & R. White) 249-300 (Springer US, 2002).
38. Kodintsev, I. M. & Trasatti, S. Electrocatalysis of H_2 evolution on RuO_2 + IrO_2 mixed oxide electrodes. *Electrochim. Acta* **39**, 1803-1808 (1994).
39. Jaramillo, T. F. et al. Hydrogen Evolution on Supported Incomplete Cubane-type $[Mo_3S_4]^{4+}$ Electrocatalysts. *J. Phys. Chem. C* **112**, 17492-17498 (2008).
40. Chen, W.-F. et al. Hydrogen-Evolution Catalysts Based on Non-Noble Metal Nickel–Molybdenum Nitride Nanosheets. *Angew. Chem. Int. Ed.* **51**, 6131-6135 (2012).
41. Bonde, J., Moses, P. G., Jaramillo, T. F., Norskov, J. K. & Chorkendorff, I. Hydrogen evolution on nano-particulate transition metal sulfides. *Faraday Discuss.* **140**, 219-231 (2008).
42. Merki, D., Vrubel, H., Rovelli, L., Fierro, S. & Hu, X. Fe, Co, and Ni ions promote the catalytic activity of amorphous molybdenum sulfide films for hydrogen evolution. *Chem. Sci.* **3**, 2515-2525 (2012).

43. Tran, P. D. et al. Novel cobalt/nickel-tungsten-sulfide catalysts for electrocatalytic hydrogen generation from water. *Energy Environ. Sci.* **6**, 2452-2459 (2013).
44. Tran, P. D. et al. Copper molybdenum sulfide: a new efficient electrocatalyst for hydrogen production from water. *Energy Environ. Sci.* **5**, 8912-8916 (2012).

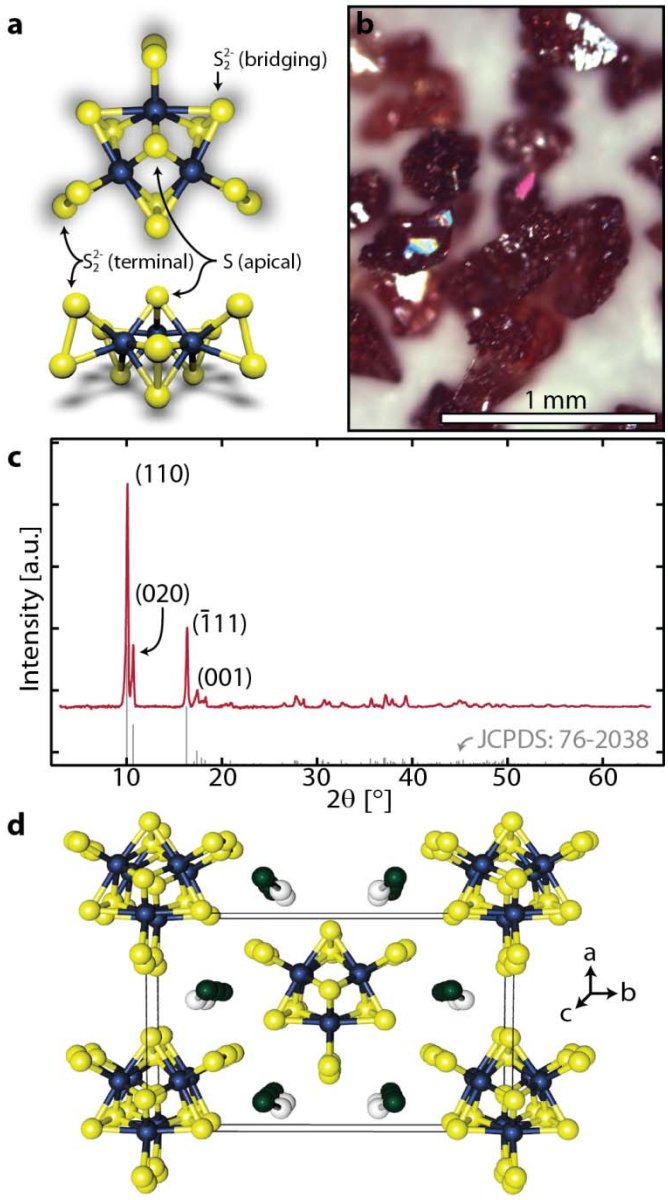

Figure 1. Structure of $[Mo_3S_{13}]^{2-}$. (a) Model of a single $[Mo_3S_{13}]^{2-}$ cluster, top and side view. (b) Optical photograph of the synthesized $(NH_4)_2Mo_3S_{13}\cdot H_2O$ crystals recorded with an Olympus BX51 microscope (brightfield). (c) Powder XRD pattern of $(NH_4)_2Mo_3S_{13}\cdot H_2O$. A simulated reference spectrum of the $(NH_4)_2Mo_3S_{13}\cdot H_2O$ crystal structure is displayed at the bottom (Joint Commission for Powder Diffraction Standards (JCPDS): #76-2038) with the corresponding $(NH_4)_2Mo_3S_{13}\cdot H_2O$ crystal structure shown in (d). Mo atoms: blue, S atoms: yellow, N atoms: green and H_2O molecules: white.

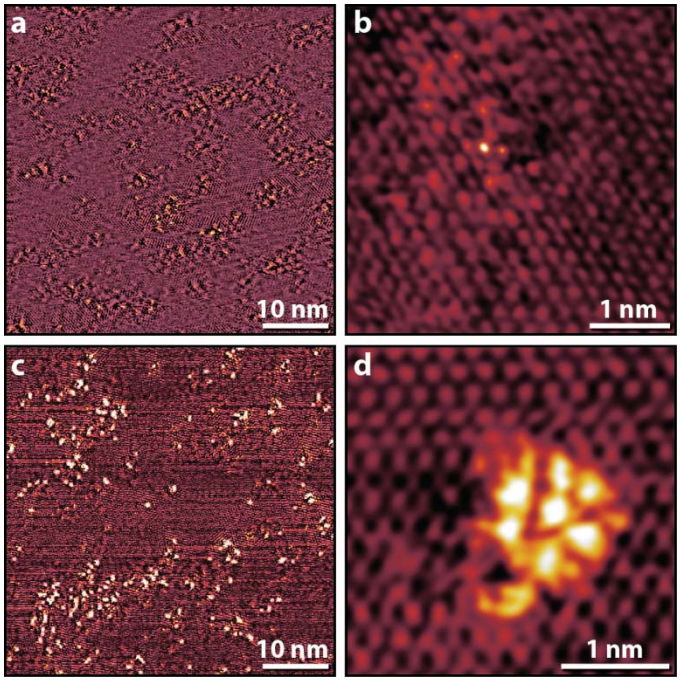

Figure 2. Atom-resolved scanning tunneling microscopy (STM). (a) Overview STM image of a bare anodized HOPG surface. (b) Atom-resolved STM image of the distorted lattice of the bare anodized HOPG surface. (c) STM image of the anodized HOPG surface after drop-casting $[Mo_3S_{13}]^{2-}$ clusters showing uniform, nanometer-sized bright protrusions. (d) Atom-resolved STM image of a single $[Mo_3S_{13}]^{2-}$ cluster revealing an ordered atomic-scale structure.

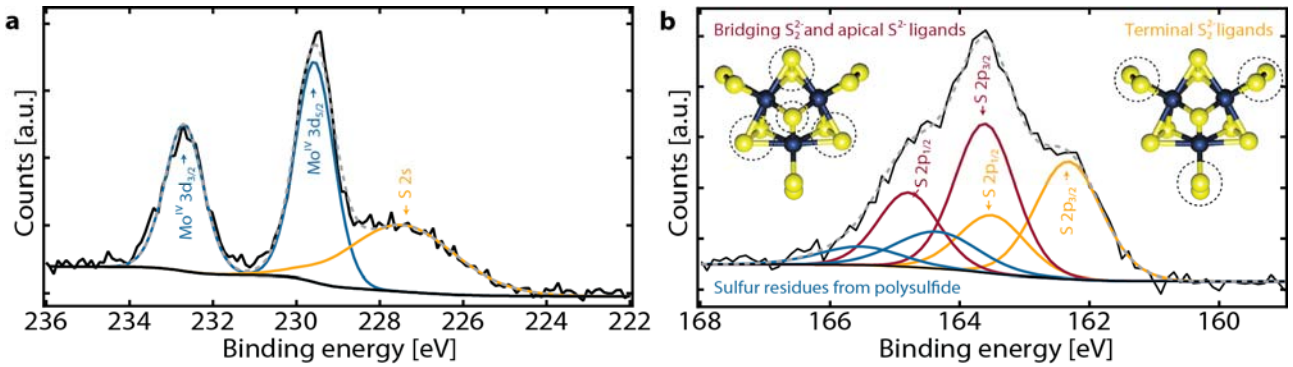

Figure 3. XPS spectra and fitted peaks of sub-monolayer $[Mo_3S_{13}]^{2-}$ clusters on HOPG. (a) Deconvolution of the Mo 3d region indicate Mo with a 4+ oxidation state. (b) The sulfur 2p region can be fitted with three district doublets ($2p_{3/2}$,$2p_{1/2}$): one doublet (in yellow) arising from the terminal S_2^{2-} ligands, one doublet (in red) reflecting the bridging S_2^{2-} ligands and the apical S^{2-} ligand of the $[Mo_3S_{13}]^{2-}$ clusters, and a doublet (in blue) at even higher binding energies accounting for residual sulfur from the polysulfide solution.

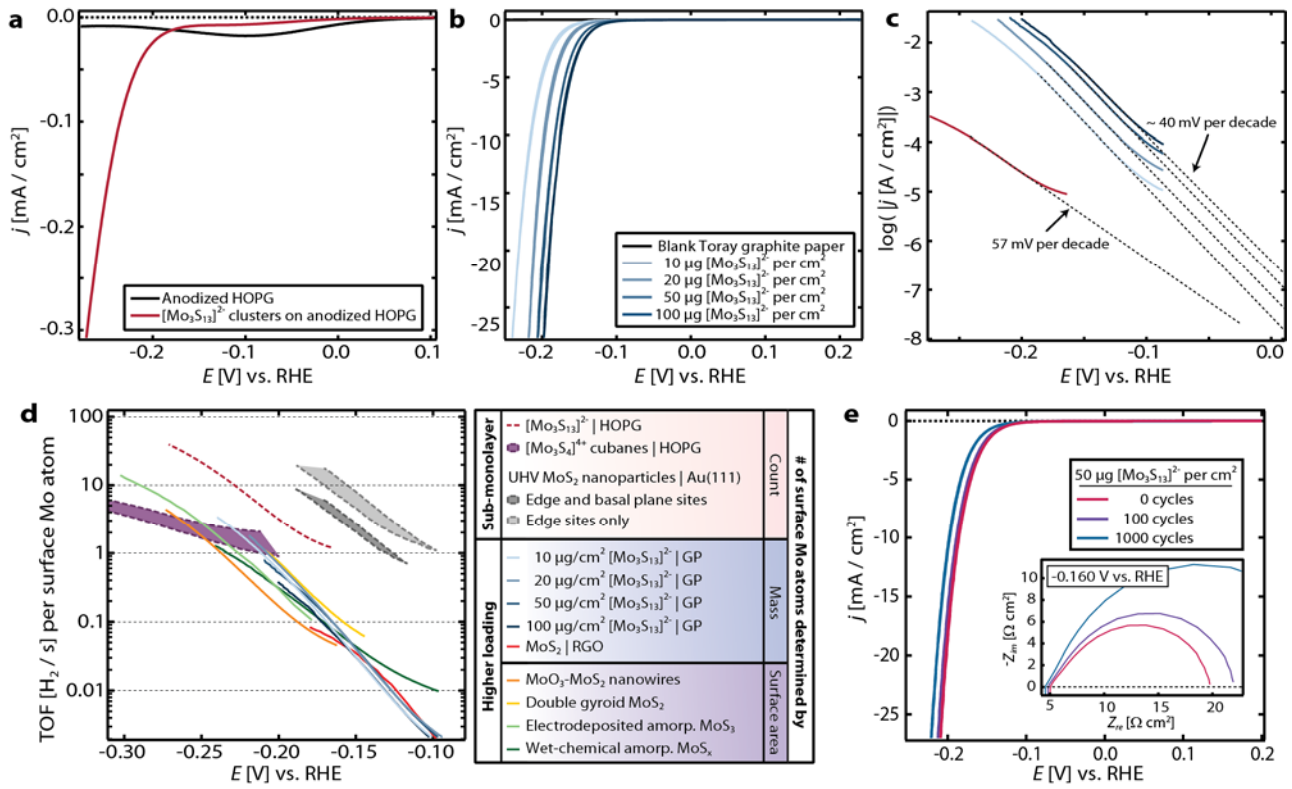

Figure 4. HER activity of $[Mo_3S_{13}]^{2-}$ clusters. (a) Polarization curve of sub-monolayer coverage of $[Mo_3S_{13}]^{2-}$ clusters on HOPG. (b). Cyclic voltammograms of $[Mo_3S_{13}]^{2-}$ clusters on Toray graphite paper (GP) with loadings of 10, 20, 50, and 100 µg per cm^2, respectively. (c) Tafel plots of the cathodic sweeps of the polarization curves in (a) and (b). See (a) and (b) for color labeling. (d) Plot displaying the turnover frequency of $[Mo_3S_{13}]^{2-}$ clusters together with several other molybdenum sulfide based HER catalysts. The $[Mo_3S_{13}]^{2-}$ clusters exhibit the highest HER turnover frequency of any molybdenum sulfide catalyst synthesized by scalable route. (e) Accelerated stability test. Initial and post potential cycling cyclic voltammograms of $[Mo_3S_{13}]^{2-}$ clusters on Toray graphite paper with a loading of 50 µg per cm^2. The inset shows the Nyquist plots of the post potential cycling impedance data. The $[Mo_3S_{13}]^{2-}$ clusters remain highly active and only a slight decrease in current density is observed upon increased potential cycling.